

Article

Numerical Simulation of Environmental Characteristics of Containment in Severe Accident of Marine Nuclear Power Plant

Zhiyong Xu , Jialei Liu, Yuqing Chen * and Ang Li

College of Nuclear Science and Technology, Naval University of Engineering, Wuhan 430033, China; m21382702@nue.edu.cn (Z.X.)

* Correspondence: chenyuqing301@163.com

Abstract: With the reliance on ocean resources, the nuclear power powers have set their sights on marine nuclear power plants to break through the bottleneck of energy supply for the development of ocean resources. In this paper, the computational fluid dynamics software ANSYS CFX 2021 is used to simulate the TOSQAN benchmark experiment. Three different turbulence models, the $k - \epsilon$ model, $RNG k - \epsilon$ model, and SST model, are selected to analyze the adaptability of the turbulence model. The simulation results are compared with the benchmark experimental results, and the selected numerical calculation model is used to analyze the influence of vapor on the pressure, temperature, hydrogen distribution, and hydrogen risk in the containment space when a hypothetical serious accident occurs in a marine nuclear power plant. The results show that the results simulated with the $k - \epsilon$ turbulence model are closer to the benchmark experimental results. Vapor has no obvious effect on the response speed of pressure balance at each position in the closed containment space, and the condensation of the vapor wall can effectively reduce the pressure peak in the closed containment space. The existence of vapor and the increase in vapor concentration will increase the temperature in the closed containment space. The condensation of vapor on the wall surface will cause the temperature in the containment space to have a peak value, which can effectively reduce the temperature in the containment space. Vapor will promote the mixing of gas in the containment space and make the hydrogen distribution tend to be uniform. The presence of vapor and the increase in vapor concentration can reduce the hydrogen risk in the containment space, but the condensation of vapor may increase the hydrogen risk in the containment space.

Keywords: marine nuclear power plant; serious accidents; containment space; numerical simulation



Citation: Xu, Z.; Liu, J.; Chen, Y.; Li, A. Numerical Simulation of Environmental Characteristics of Containment in Severe Accident of Marine Nuclear Power Plant. *Energies* **2023**, *16*, 7821. <https://doi.org/10.3390/en16237821>

Academic Editors: Alessandro Del Nevo and Andrey A. Kurkin

Received: 28 August 2023

Revised: 7 November 2023

Accepted: 17 November 2023

Published: 28 November 2023



Copyright: © 2023 by the authors. Licensee MDPI, Basel, Switzerland. This article is an open access article distributed under the terms and conditions of the Creative Commons Attribution (CC BY) license (<https://creativecommons.org/licenses/by/4.0/>).

1. Introduction

Marine nuclear power plants have the advantages of high efficiency and economy, which can bring considerable economic benefits to some remote coastal areas lacking resources, and are considered the most ideal energy guarantee for marine development. The containment of marine nuclear power plants mainly has two design schemes: square and cylindrical [1–3]. Compared with the square, the cylindrical containment has high space utilization, good structural stability, and strong compression resistance, which provides good protection for nuclear reactors and can be used for deep sea exploration and the development of seabed resources [4]. Marine nuclear power plants generally use small pressurized water reactors with relatively mature technology. However, in the process of serious accidents induced by the loss of coolant accident, the pressurized water reactor will produce chemically active hydrogen [5,6], which is released into the containment with vapor through the pipeline break or safety valve and mixed with the air in the containment space. When the mixture of hydrogen, air, and vapor reaches a certain proportion, the risk of hydrogen combustion or even explosion may occur under appropriate conditions, and a high-pressure peak will be formed in the containment space in a very short time. The resulting static and dynamic pressure loads will threaten the integrity of the containment

and affect the integrity of the internal facilities of the containment, posing a serious threat to the safety of the reactor. The Fukushima nuclear accident in 2011 was due to the hydrogen accumulation explosion, which destroyed the integrity of the reactor building structure, caused a large number of radioactive substances to be released into the environment, and brought a series of problems to the accident emergency rescue [7,8].

Research institutions around the world have conducted experimental studies on the hydrogen risk in small pressurized water reactors and containment space after accidents, which has enhanced the predictability and controllability of accidents. German research institutions have studied the effect of natural circulation on hydrogen transport using the BMC PWR containment experimental facility [9]. France's CEA (Commissariat à l'énergie atomique et aux énergies alternatives) used MISTRA experimental facilities to study the coupling effect between the transport of mixed gas composed of hydrogen, vapor, and air and wall condensation and analyzed the transient behavior of mixed gas transport and the concentration distribution of steady-state gas [10]. The French IRSN (Institut de Radioprotection et de Sécurité Nucléaire) used a small single-chamber experimental facility TOSQAN to study the effects of injection conditions, condensation, and spray on hydrogen stratification and mixing [11,12], analyzed the natural circulation phenomenon under different gas composition conditions [13], and used the device to study the establishment and transport behavior of hydrogen stratification at the top of the container [14]. German research institutions have studied the coupling effects between natural circulation, condensation, and hydrogen transport, as well as the effects of jet, natural circulation, and gas radiation on hydrogen transport using the multichambered coupling effect experimental facility THAI [15,16]. The Indian Institute of Technology used a small experimental facility, AIHMS, to study the effects of wall temperature-driven natural circulation and obstacles on gas mixing [17,18]. However, due to the use of helium instead of hydrogen in the experiment, these experimental studies lack the analysis of possible hydrogen risks. With the development of computer resources, numerical simulation through computer simulation platforms has become an important means of hydrogen risk research in containment. Filippov and Bakhmet'ev et al. verified the relevant models in FLUENT and KUPOL-MT programs [19,20]. Fernández-Cosials et al. used the IBE-3 experiment at the PANDA experimental facility to verify the GOTHIC program based on the gas mixing process [21]. Kelm et al.'s experimental data based on THAI and MISTRA facilities used CFX to predict the gas mixing process [22]. Povilaitis et al. predicted the experimental phenomena in the MISTRA facility using a one-dimensional COCOSYS program [23]. Based on the experimental results of THAI-HM2, Visser et al. analyzed the sensitivity of the turbulence model and related parameters by FLUENT [24]. These numerical simulations use experimental data to verify the model of the software, but there is a lack of further analysis of the effect of water vapor on hydrogen distribution.

From the analysis of the above studies, it can be seen that the hydrogen risk studies for the containment of small pressurized water reactors are mainly based on land-based reactors. However, compared with land-based nuclear power plants, marine nuclear power plants need to face the complex marine environment, harsh operating conditions, and the ultimate heat sink is the sea. Although it can provide a good source of continuous cooling, the space of the containment of marine nuclear power plants is smaller, and the amount of vapor condensation during serious accidents is large, which increases the hydrogen concentration in the containment space and destroys the steam inert environment in the containment space, thus making the containment space of marine nuclear power plants more prone to hydrogen combustion and even explosion risks. Therefore, it is necessary to analyze the impact of vapor generated during the severe accident of marine nuclear power plants on the hydrogen risk in the containment space.

In this paper, the computational fluid dynamics software CFX is used to simulate the TOSQAN benchmark experiment in the international benchmark problem ISP-47 of containment thermal hydraulics. The simulation results are compared with the experimental results to verify the applicability of the selected numerical calculation model. Then, a sim-

plified three-dimensional geometric model of the containment space of a cylindrical marine nuclear power plant is established. The selected calculation model is used to simulate and analyze the influence of vapor sprayed from the nozzle on the pressure, temperature, hydrogen distribution, and hydrogen risk in the containment space during the serious accident induced by the hypothetical loss of coolant in the marine nuclear power plant, which provides a reference for the subsequent hydrogen risk analysis under the serious accident of the marine nuclear power plant.

2. Physical Model

The gas produced in the process of a serious accident is sprayed into the containment from the breach and continuously moves in the containment space under the action of inertial force and buoyancy force. In this process, gas concentration diffusion, turbulent diffusion, convection, and vapor condensation play a major role, accompanied by heat transfer. This process can be approximately simulated by solving the following control equations and model settings in CFD.

2.1. Governing Equation

The governing equations are mainly used to solve the multicomponent gas flow and heat transfer process in the containment space of marine reactors during severe accidents, including the mass equation, momentum equation, energy equation, and component transport equation.

Mass conservation equation:

$$\frac{\partial \rho}{\partial t} + \nabla \cdot (\rho U) = S_M \quad (1)$$

Momentum conservation equation:

$$\frac{\partial (\rho U)}{\partial t} + \nabla \cdot (\rho U \otimes U) = \nabla \cdot \Gamma + \nabla \cdot \tau + \rho f + S_U \quad (2)$$

Energy conservation equation:

$$\frac{\partial (\rho E)}{\partial t} + \nabla \cdot (\rho U E) = \nabla \cdot (\lambda \nabla T) + \rho f \cdot U + \nabla \cdot (\Gamma \cdot U) + \nabla \cdot (\tau \cdot U) + S_E \quad (3)$$

Species equation:

$$\frac{\partial (\rho \omega)}{\partial t} + \nabla \cdot (\rho U \omega) = \nabla \cdot (\rho D \nabla \omega) + S_M \quad (4)$$

where t is time, unit s; ρ is the density, unit kg/m³; U is the speed, unit m/s²; E is energy, unit J; T is temperature, unit K; Γ is the surface force, unit N/m²; f is the volume force, unit N/m²; τ is the stress tensor, unit Pa; λ is the thermal conductivity, unit W/(m·K); S_M is the mass source term, unit kg/(m³·s); S_U is the momentum source term, unit N/m³; S_E is the energy source term, unit J/(m³·s); D is the diffusion coefficient, unit m²/s; ω is the mass fraction.

2.2. Buoyancy Force Model

Buoyancy is caused by the change in density, and the change in density may come from the change in local temperature, the change in mass fraction in the multicomponent flow, the difference in density between phases in the multiphase flow, and the change in local pressure of the ideal gas and the actual fluid. In the CFX software, the influence of the buoyancy effect on the flow process is realized by adding the buoyancy source term shown in Equation (5) to the momentum equation:

$$S_{M,buoy} = (\rho - \rho_{ref}) \vec{g} \quad (5)$$

where ρ is the fluid density, unit kg/m^3 ; ρ_{ref} is the reference density, unit kg/m^3 ; \vec{g} is the gravitational acceleration vector, unit m/s^2 .

CFX software provides two different buoyancy models, which are the Boussinesq model and the full buoyancy model. The former is mainly used for the case where the fluid is not a function of pressure and temperature. The latter is mainly used for multicomponent flow, multiphase flow, and fluid flow, where density is a function of pressure, temperature, or other field variables. Therefore, the full buoyancy model is used in this paper.

2.3. Wall Condensation Model

The CFX program has developed a special wall condensation model for the containment of nuclear power plants, which is mainly used to simulate the condensation of condensable components in variable component mixtures (such as vapor and air). In this model, the condensation of vapor in the variable component mixture is driven by the concentration gradient of vapor near the wall. The internal boundary mass source is used to simulate the amount of condensed water removed from the system, ignoring the thickness of the condensate film and the heat transfer through the condensate film. The mass flux of vapor at the gas–liquid interface is determined by the molar fraction of dry vapor by assuming that the liquid film at the gas–liquid interface is in thermal equilibrium.

For turbulent flow, the wall condensation model uses the turbulent wall function to model the concentration boundary layer. In a turbulent boundary layer, the molar fluxes of the non-condensable component A and the condensable component B are J_A and J_B , respectively, for a binary gas mixture passing through a plane parallel to the wall and at a distance of y from the wall boundary, from the conservation of mass, it can be obtained:

$$J_{Aw} = J_m X_{Aw} - T_M (X_{AP} - X_{Aw}) = 0 \text{ (non-condensable)} \quad (6)$$

$$J_{Bw} = J_m X_{Bw} - T_M (X_{BP} - X_{Bw}) \text{ (condensable)} \quad (7)$$

where the subscript w represents the wall; the subscript P denotes the near-wall grid points; T_M is the wall multiplier determined by the turbulent wall function; X_A and X_B are the molar fractions of non-condensable component A and condensable component B , respectively.

Since component A is not condensable, $J_{Bw} = J_{Bm}$. The condensation molar flux of the condensable component B is obtained by adding Formulas (6) and (7) and combining the constitutive relation $X_A + X_B = 1$:

$$J_{Bm} = -T_M \frac{X_{BP} - X_{Bw}}{1 - X_{Bw}} \quad (8)$$

Since the mass fraction is required in the multicomponent flow model, Equation (8) is transformed into the mass fraction form:

$$M_{Bm} = -T_M \frac{Y_{BP} - Y_{Bw}}{1 - Y_{Bw}} \quad (9)$$

where Y represents the mass fraction, the value of Y_{BP} is obtained from the transport equation of the condensable component B , and the value of Y_{Bw} is calculated from the molar fraction of the condensable component B .

3. Numerical Calculation Model Verification

Three different turbulence models are used to simulate the TOSQAN benchmark experimental conditions in the ISP-47 international benchmark problem of containment thermal hydraulics. The simulated local field distribution, including gas velocity, gas temperature, and hydrogen (helium) and vapor concentration distribution, is compared with the experimental results to verify the applicability of the selected CFX calculation

model to simulate the hydrogen distribution in the containment space during the severe accident of marine nuclear power plants.

3.1. TOSQAN Experimental Device

The TOSQAN experimental device is a small single-chamber closed container with an internal volume of 7 m^3 , which is composed of a cylindrical stainless steel chamber and a sink. The constant temperature control of the container wall is realized by external oil injection. There is a cylindrical 'cold wall' with a height of 2 m inside, and a lower temperature is applied to form a condensation wall. The experimental gas is injected into the container through a vertical pipe with a diameter of 41 mm on the central axis of the container, as shown in Figure 1. Due to the chemical properties of hydrogen being more active, for safety considerations, inert helium gas was used instead of hydrogen in the experimental process for testing [25].

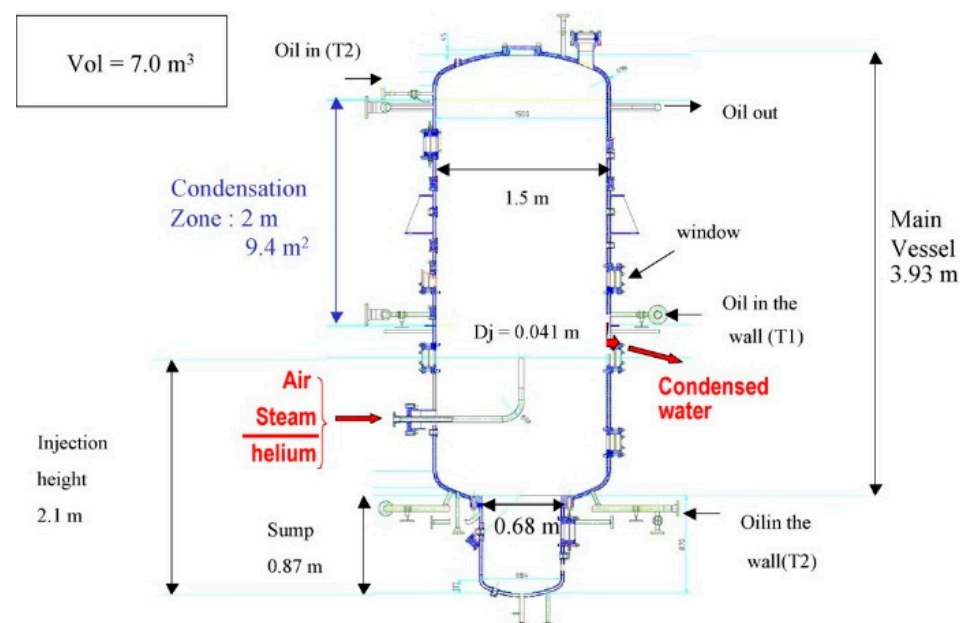


Figure 1. Size diagram of TOSQAN experimental device.

The TOSQAN benchmark test consists of a series of different steady-state conditions. These steady-state conditions are obtained by changing the injection conditions so that the steam condensation rate is equal to the steam injection rate. Each steady-state condition maintains different constant boundary conditions, especially the wall temperature and the steam injection mass flow rate. The initial conditions and boundary conditions during the experimental test are described in reference [11].

3.2. Geometric Model and Mesh Division

This paper uses simulation software (ANSYS CFX 2021) to numerically simulate the experiment. The external boundary conditions during the experiment can be set by the software, so the external facilities of the experimental device are not considered in the geometric modeling process. Figure 2a is a geometric model of the internal space of the experimental device established by using the three-dimensional modeling software Solidworks 2018 according to the size diagram of the TOSQAN experimental device.

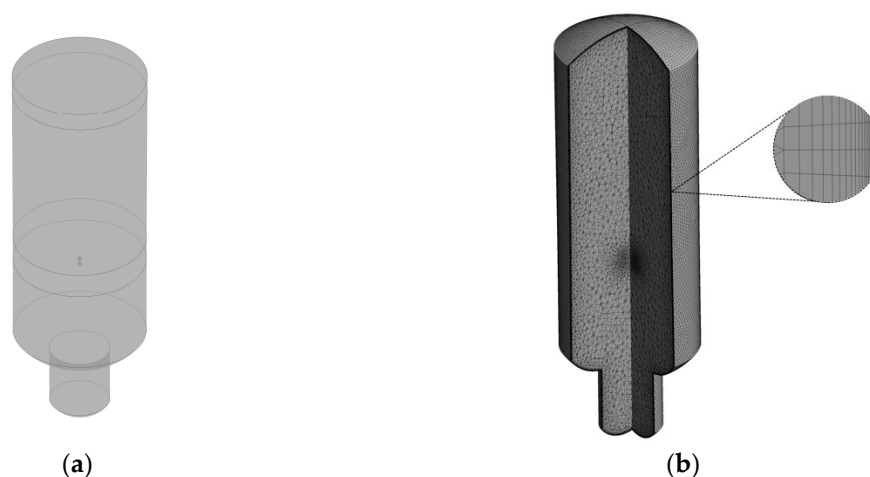


Figure 2. Geometric and Mesh models of TOSQAN experimental device. (a) Geometric model. (b) Mesh division.

The geometric model is divided into unstructured grids by the Workbench mesh. During the experimental test, the vapor will condense near the cold wall, and the grids near the wall will affect the prediction accuracy of the local field. Therefore, it is necessary to divide the boundary layer into a geometric model. According to reference [26], when the total thickness of the boundary layer is 30 mm, and the number of layers exceeds 10, the mesh size near the wall can meet the requirements of mesh independence. In this paper, the geometric model of the experimental device is divided into unstructured grids. Considering the prediction accuracy of the local field and the computing resources, the number of boundary layers is divided into 15 layers under the premise that the total thickness of the boundary layer is 30 mm, as shown in Figure 2b. Table 1 shows five sets of unstructured grids with different element numbers obtained by changing the unit size of the volume grid under the premise of maintaining the consistency of the boundary layer grids. The grid independence analysis is performed using these five sets of grids. The results are shown in Figure 3. By comparing the results of the hydrogen molar fraction distribution calculated by different grid division schemes, it can be seen that the radial distribution trends of the hydrogen molar fraction calculated by the grid division scheme with the size of 0.035 m, 0.03 m, and 0.025 m are the same. The maximum deviation between the three grid calculation results is about 1.81%, which meets the requirements of grid independence. Therefore, considering the prediction accuracy, computing resources, and efficiency, this paper chooses the grid division scheme with a size of 0.03 m to simulate the benchmark experiment.

Table 1. Meshing scheme of the geometric model of TOSQAN experimental device.

Total Elements	Total Nodes	Mesh Size	Maximum Skewness	Average Skewness	Standard Deviation
632,653	243,085	0.045	0.78455	0.14952	0.11938
802,246	307,848	0.04	0.80993	0.14778	0.11980
1,046,878	403,067	0.035	0.81553	0.14652	0.12140
1,438,922	550,412	0.03	0.83569	0.14707	0.12208
2,120,164	802,898	0.025	0.84632	0.14697	0.12245

In this paper, the transient calculation method is used to simulate the benchmark experiment. The size of the time step in the transient calculation process will affect the convergence of the calculation and the calculation results. Therefore, it is necessary to analyze the independence of the time step. Using the above-determined meshing scheme, the hydrogen molar fraction distribution results obtained by changing the time step size only under the premise of keeping the initial conditions and boundary conditions unchanged

are shown in Figure 4. From the diagram, it can be seen that the changing trend in the radial distribution of hydrogen molar fraction calculated by the time step of 0.05 s, 0.01 s, and 0.005 s is the same. The maximum deviation between the calculation results of the three time steps is about 0.24%, which meets the requirement of time step independence. Continuing to reduce the time step has no significant improvement in calculation accuracy. Therefore, this paper selects a time step of 0.01 s to perform the transient simulation on the benchmark experiment.

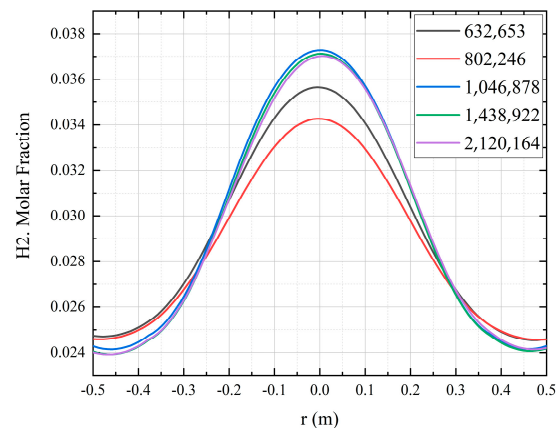


Figure 3. TOSQAN geometric model mesh influence analysis.

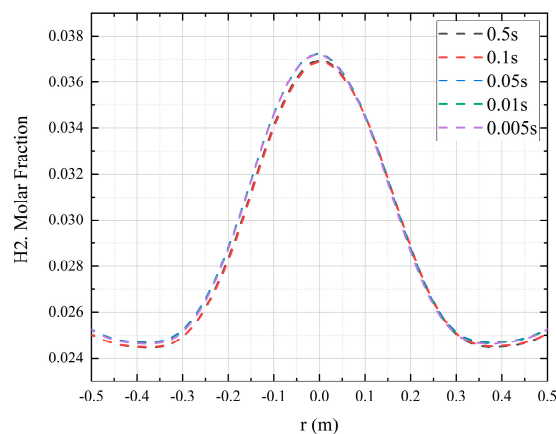


Figure 4. Time step analysis of TOSQAN geometric model.

3.3. Adaptability Analysis of Turbulence Model

The purpose of this paper is to study the effect of vapor on the hydrogen risk in the containment space during a severe accident at a marine nuclear power plant. Therefore, the experimental data of the fourth steady-state condition in the TOSQAN benchmark experiment are used to verify the numerical model. Based on the grid division scheme and time step determined by grid independence verification and time step independence analysis, according to the initial conditions and boundary conditions of the experimental test in the literature [11], the $k - \epsilon$ model, SST model, and RNG $k - \epsilon$ model are used respectively. Three different turbulence models were used to simulate the benchmark experimental process. The comparison of the flow velocity, temperature, and hydrogen and vapor concentration distribution obtained by the three turbulence models with the experimental data is shown in Figure 5. The average deviation between the simulated and

experimental values of these three turbulence models was calculated using the following equation as a basis for turbulence model selection:

$$\frac{1}{n} \sum \left(\frac{x - y}{y} \right) \quad (10)$$

where x represents the simulated values; y represents the experimental values; n represents the number of experimental values.

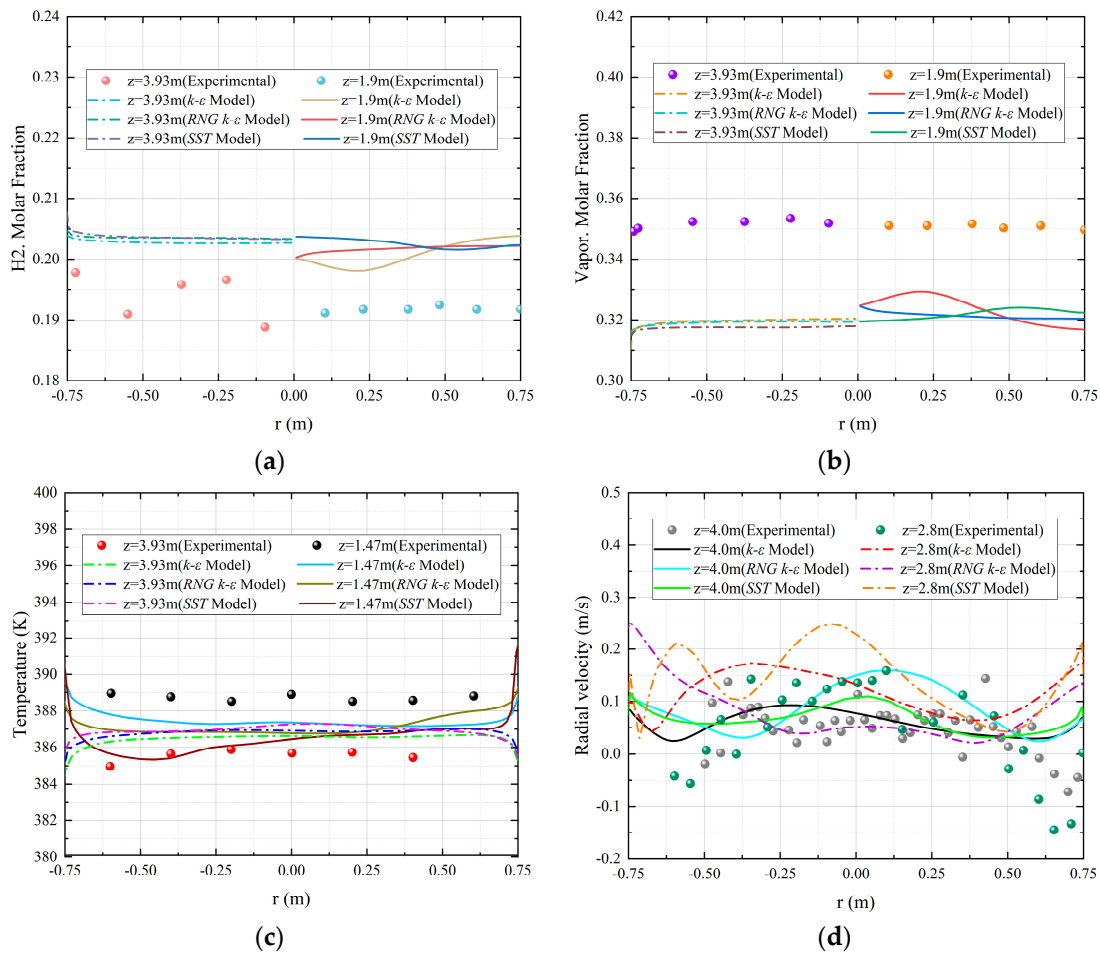


Figure 5. Comparison of numerical simulation results with experimental values. (a) Comparison of hydrogen concentration distribution. (b) Comparison of vapor concentration distribution. (c) Comparison of temperature distribution. (d) Comparison of velocity distribution.

The average deviations between the simulated and experimental values of the radial hydrogen molar fraction, radial water vapor molar fraction, and radial temperature at different elevations calculated by the $k-\epsilon$ turbulence model are about 7.37%, 8.33%, and 0.47%, respectively. The average deviations between the simulated and experimental values of the radial hydrogen molar fraction, radial vapor molar fraction, and radial temperature at different elevations calculated by the RNG $k-\epsilon$ turbulence model are about 9.89%, 10.21%, and 0.74%, respectively. The average deviations between the simulated and experimental values of the radial hydrogen molar fraction, radial vapor molar fraction, and radial temperature at different elevations calculated by the SST turbulence model are about 10.23%, 10.69, and 2.55%, respectively. However, the errors between the simulated and experimental values of the three turbulence models for the local field of velocity are relatively large. The main reason is that in the process of geometric modeling of the experimental device, the complex auxiliary structures in the actual device are ignored.

These structures will affect the diffusion of gas, resulting in the deviation between the experimental value and the simulated value. In general, the simulation results of the $k - \varepsilon$ turbulence model are in good agreement with the experimental data compared with the other two turbulence models, which indicates that the $k - \varepsilon$ turbulence model has better adaptability to simulate the hydrogen distribution in the closed space. Therefore, in this paper, the $k - \varepsilon$ turbulence model is selected for the subsequent simulation calculation in the closed containment space of the marine nuclear power plant.

4. Containment Space Model

4.1. Geometric Model and Mesh Division

In the process of severe accidents in marine nuclear power plants, the gas mixture is sprayed and released vertically upwards into the containment space and flows and spreads in the containment gas space. In the process of movement, it will come into contact with the wall surface of the containment and other equipment components, but the wall surface of the complex equipment components does not come into direct contact with the seawater, and it does not have much effect on the pressure and temperature changes in the containment space. Due to the special characteristics of the operating environment and usage requirements, the actual arrangement of the equipment and components in the containment should be very compact. Moreover, in the process of gas mixture spraying in a serious accident, due to the large initial momentum of the sprayed gas mixture, the gas stirring effect on the gas in the space of the containment is large, which will promote the flow of the gas, and therefore, the possibility of localized gathering of hydrogen in the process of a serious accident is low. Therefore, the rest of the equipment and components in the containment space have a certain influence on the size of the concentration stratification area formed by hydrogen, but they do not have a greater influence on the size of the hydrogen concentration in each concentration stratum and the distribution trend of the hydrogen concentration stratum. These equipment and components have a greater influence on the size of the concentration stratification area formed by hydrogen. Moreover, these equipment and components are more often distributed in the lower region of the containment, while hydrogen, as a less dense gas, tends to be distributed in the upper space of the containment. Therefore, it is feasible to ignore the rest of the equipment and components inside the containment. So, we have adopted a simplified containment model for the simulation of the containment of an offshore nuclear power plant.

A simplified geometric model of a long cylindrical containment of a marine nuclear power plant with an inner diameter of 4.5 m and a length of 5.6 m was established by using three-dimensional modeling software. The inner surface of the bottom of the containment was used as the reference elevation (+0 m). At the center of the elevation of +1.73 m (vertical upward), the source term gas entered the containment space through the incident pipeline. Five hypothetical measuring points were set at different elevations in the containment space to analyze the change of the local field with time, as shown in Figure 6.

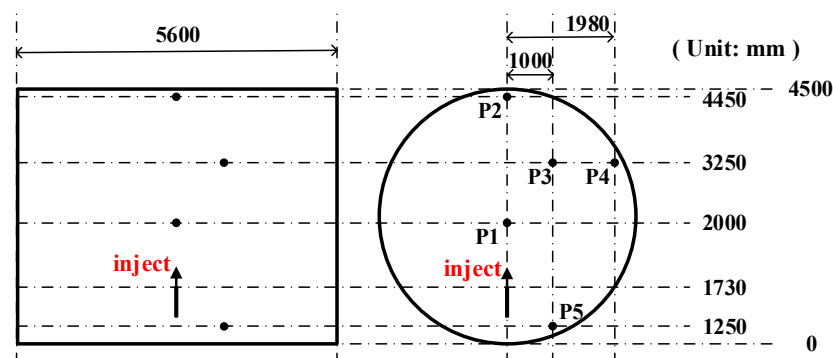


Figure 6. Dimensions of the geometric model of the containment and schematic diagram of the local field measurement points.

The established geometric model is divided into unstructured grids. The total thickness of the boundary layer grid is 0.03 m, and the number of layers is 15, as shown in Figure 7. Keeping the boundary layer mesh unchanged and changing the size of the volume mesh of the containment geometry model, five sets of meshing schemes with different mesh element numbers are obtained, as shown in Table 2. The grid independence analysis is carried out by using these five sets of grids, and the results are shown in Figure 8. Comparing the results obtained by different grid calculations, it can be seen that the radial distribution trend of the hydrogen molar fraction in the containment space calculated by the volume grid size of 0.1 m, 0.08 m, and 0.06 m is the same, and the maximum deviation is about 1.47%. Increasing the number of grids is not obvious to improve the calculation accuracy and meet the requirements of grid independence. Therefore, considering the calculation accuracy, computing resources, and efficiency, this paper chooses the grid division scheme with a volume grid size of 0.08 m to carry out the numerical simulation of the containment space geometric model of the marine nuclear power plant.

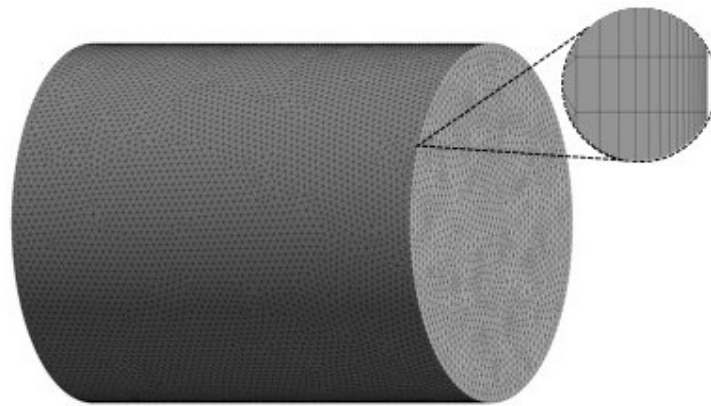


Figure 7. Mesh generation of containment geometry model.

Table 2. Containment geometry model meshing scheme.

Total Elements	Total Nodes	Mesh Size	Maximum Skewness	Average Skewness	Standard Deviation
270,759	80,041	0.2	0.79292	0.20843	0.13136
382,616	124,234	0.15	0.79230	0.19508	0.13447
746,789	261,168	0.1	0.84889	0.18221	0.13024
1,127,714	399,741	0.08	0.82073	0.17435	0.12857
2,016,072	710,252	0.06	0.81322	0.16598	0.12533

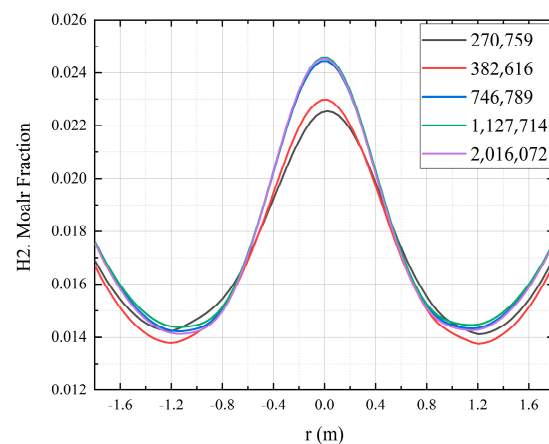


Figure 8. Grid independence analysis of containment geometry model.

4.2. Initial Conditions and Basic Assumptions

This paper mainly focuses on the influence of vapor emitted from the break on the pressure, temperature, hydrogen distribution, and hydrogen risk in the containment space under the severe accident of a marine nuclear power plant. Using the same model setting as the above simulated TOSQAN benchmark experiment, and using the $k - \epsilon$ turbulence model, the existence of vapor, vapor concentration, and the influence of vapor condensation are analyzed. The specific calculation parameters are shown in Table 3. In the simulation process, the geometric model of the containment wall is assumed to be a constant temperature boundary condition; the temperature difference between the inner and outer walls is 25 °C, and the wall boundary is a non-slip boundary condition. The space condensation of vapor and radiation heat transfer is not considered.

Table 3. Initial conditions and boundary conditions.

Parameters	Case 1	Case 2	Case 3	Case 4
vapor mass flow rate / $\text{kg}\cdot\text{s}^{-1}$	0	0.08	0.16	0.08
hydrogen mass flow rate / $\text{kg}\cdot\text{s}^{-1}$	0.002	0.002	0.002	0.002
injection temperature /°C	230	230	230	230
injection time /s	800	800	800	800
dwel time /s	200	200	200	200
jet size /mm	38	38	38	38
initial gas composition	Air	Air	Air	Air
initial temperature /°C	25	25	25	25
initial pressure /Mpa	0.1	0.1	0.1	0.1
wall temperature /°C	50	50	50	adiabatic

Because the transient calculation method is used to simulate the above conditions, it is necessary to analyze the independence of the time step. Based on the grid division scheme determined by grid independence analysis, different time steps are used for calculation, and the results are shown in Figure 9. Comparing the calculation results of different time steps in the figure, it can be seen that the changing trend of the hydrogen molar fraction in the containment space with the radial position calculated by time steps of 0.05 s, 0.01 s, and 0.005 s is the same, and the maximum deviation is about 1.08%, which meets the requirement of the time step independence of transient calculation. Therefore, this paper selects the 0.01 s time step to calculate the transient condition in the containment space of the marine nuclear power plant.

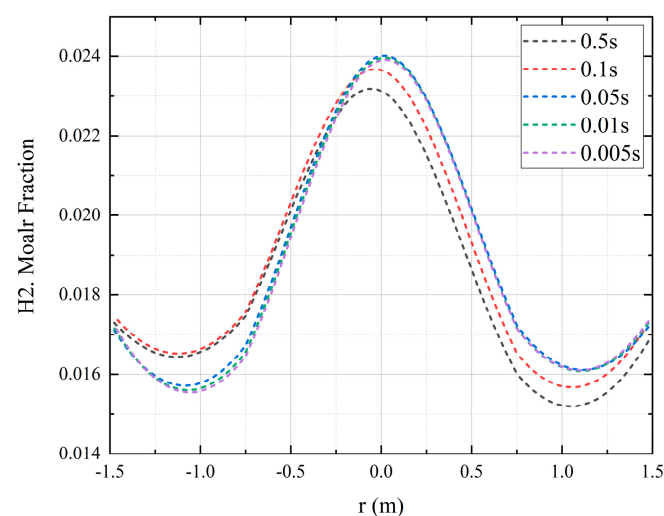


Figure 9. Time step independence analysis of containment geometry model.

5. Numerical Simulation Results Analysis

5.1. Analysis of the Influence of Vapor

Figure 10a–c is the dynamic change of the average pressure in the containment space and the pressure at different positions under the conditions without vapor and vapor, respectively. From Figure 10a,b, it can be seen that the changing trend of the average body pressure in the containment space with time under the two working conditions during the whole accident process is completely consistent with the changing trend at each measuring point. This shows that the pressure response in the containment space of the floating nuclear power plant with limited closed volume is very rapid, regardless of whether there is vapor in the mixed gas sprayed from the break during the accident so that the pressure at each point in the containment space quickly reaches equilibrium. However, compared with the condition without vapor injection, the pressure in the containment space under the condition of vapor injection is relatively high during the whole accident process, as shown in Figure 10c. The main reason is that the high-temperature vapor and hydrogen are injected into the closed containment together from the nozzle during the accident, which makes the pressure in the containment space rise.

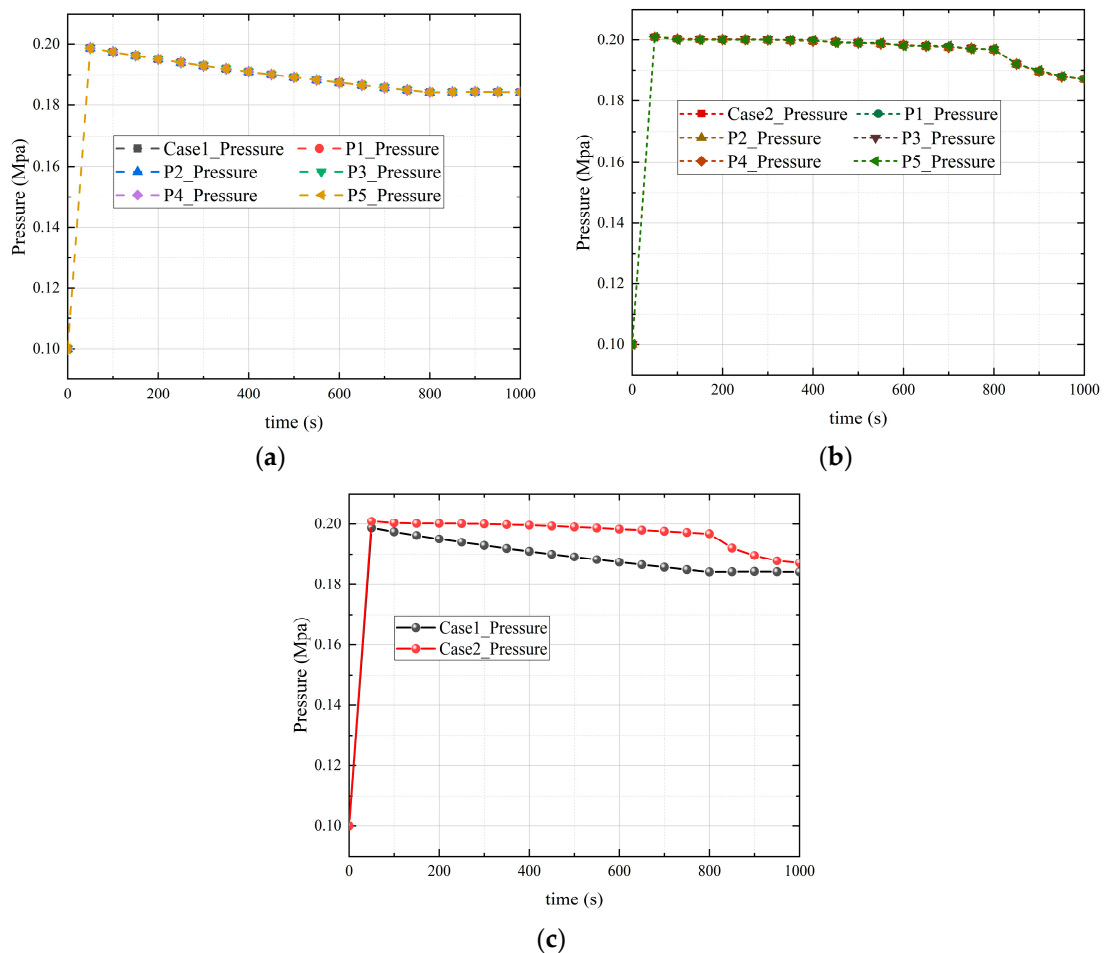


Figure 10. Pressure change in the containment space under different working conditions. (a) Pressure change of Case 1. (b) Pressure change of Case 2. (c) Average pressure change of Case 1 and Case 2.

Figure 11 shows the comparison of the average temperature in the containment space under the condition without vapor and the condition with vapor. It can be seen from the figure that during the accident, the temperature in the containment space under the condition of no vapor continues to rise with time until the end of the gas injection. Under the condition of vapor, the temperature in the containment space rises to about 700 s and

reaches the peak value, and the overall change gradient of temperature is larger than that without vapor. The main reason for this phenomenon is that under the condition of vapor, the vapor is mixed with hydrogen from the nozzle and sprayed into the containment space. The addition of vapor increases the initial velocity of the mixed gas sprayed from the nozzle, and the amount of high-temperature gas sprayed into the containment space at the same time is greater, which makes the temperature in the containment space higher. At the same time, the initial momentum of the high-temperature mixed gas is larger, and the diffusion distance in the containment space is farther at the same time, thus promoting heat transfer in the containment space.

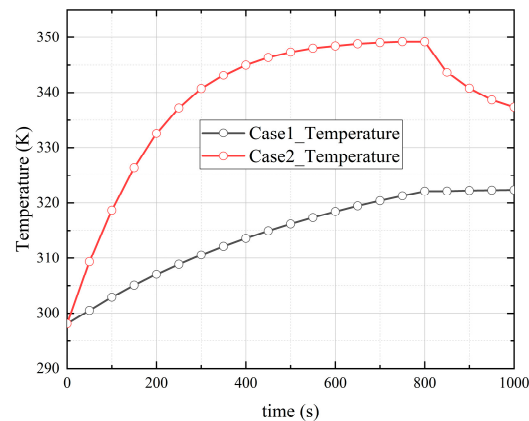


Figure 11. Average temperature change of Case 1 and Case 2.

Figure 12 shows the dynamic change of the hydrogen molar fraction at the P1 measuring point near the nozzle in the containment space under these two conditions. It can be seen from the figure that the change in the hydrogen molar fraction at the P1 measuring point with time is the same under the two working conditions during the whole accident process. However, in the stage of concentrated gas injection, the hydrogen molar fraction at the P1 measuring point under the condition of vapor injection is much lower than that under the condition of no vapor injection, and the minimum reduction is about 77.17%. The main reason for the large difference in the hydrogen molar fraction at the same time point and position under these two working conditions is that in the process of vapor and hydrogen being injected into the containment space from the nozzle under the vapor injection condition, the vapor will have an entrainment effect on hydrogen, and the diffusion of vapor in the containment space will enhance the disturbance to the original gas environment in the space, thus promoting the mixing and diffusion of gas in the containment space, as shown in Figure 13. Figures 14 and 15 show the comparison of the streamline diagram and the hydrogen distribution cloud diagram at the same time under different working conditions, which can more intuitively show the enhancement of the effect of vapor injection on the gas environment disturbance in the containment space during the concentrated gas release stage. From the diagram, it can be seen that during the period of gas-concentrated injection, the vortex formed in the containment space of the working condition with vapor injection is larger and faster in speed, which makes the hydrogen concentration distribution in this stage relatively uniform. The variation in the hydrogen molar fraction in the containment space in the gravitational direction at the moment of $t = 800$ s, shown in Figure 16 further demonstrates that in the case of vapor injection, there is no obvious hydrogen concentration gradient in the containment space at the stage of gas injection and the distribution is relatively homogeneous, whereas in the case without vapor injection, there is a large and obvious hydrogen concentration gradient in the containment space.

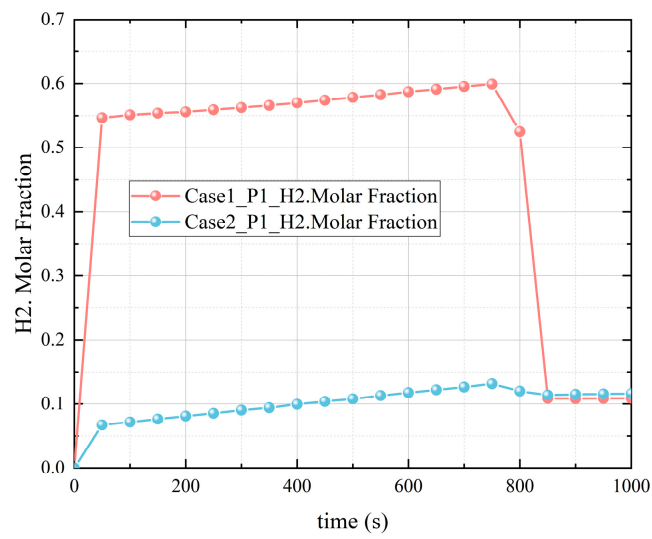


Figure 12. Change of hydrogen concentration at P1 measuring point in Case 1 and Case 2.

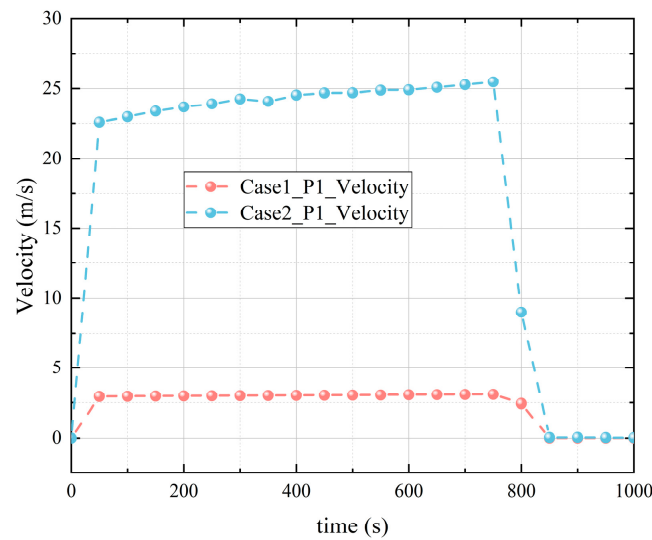


Figure 13. Velocity change at P1 measuring point in Case 1 and Case 2.

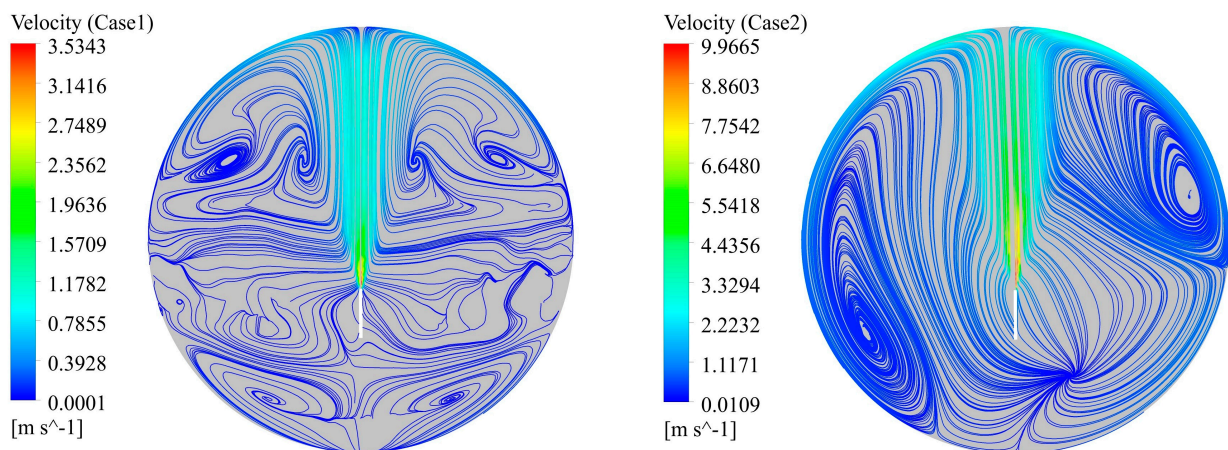


Figure 14. Streamline diagram under different working conditions at t = 800 s (left) Case 1; (right) Case 2.

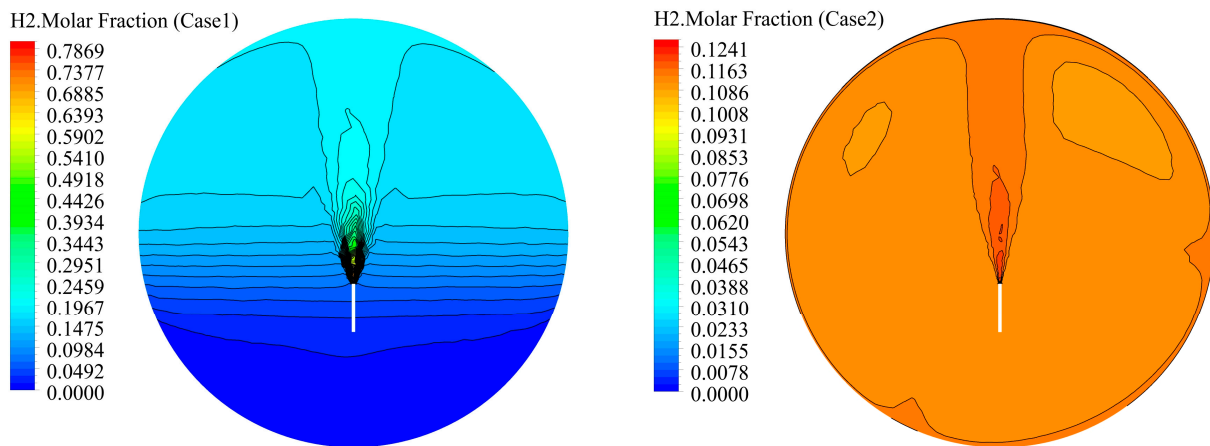


Figure 15. Distribution of hydrogen concentration under different working conditions at $t = 800$ s (left) Case 1; (right) Case 2.

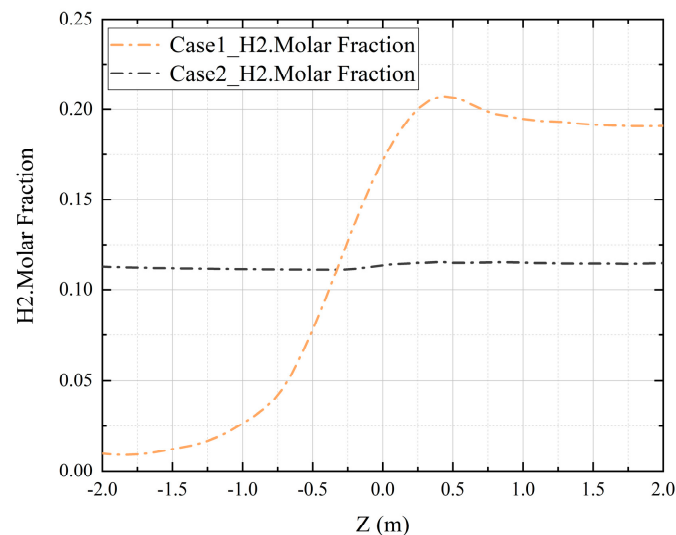


Figure 16. Change of gravity hydrogen concentration under different working conditions at $t = 800$ s ($r = 0.15$ m).

5.2. Analysis of the Influence of Vapor Concentration

Figure 17a shows the dynamic changes of pressure at different positions in the containment space under the condition of large vapor mass flow. It can be seen from the figure that the changing trend in the average pressure in the containment space with time under the whole accident process is completely consistent with the changing trend in the pressure at each measuring point, which indicates that under the condition of large vapor concentration, the pressure response in the containment space during the accident of the floating nuclear power plant with limited closed volume is also very rapid so that the pressure at each point in the space quickly reaches the equilibrium state. However, the average body pressure in the containment space is higher during the whole accident process under the condition of large steam mass flow, as shown in Figure 17b. This is mainly due to the large amount of high-temperature vapor sprayed from the nozzle into the containment space at the same time under the condition of large vapor mass flow (as shown in Figure 18), which makes the pressure in the closed containment space increase greatly.

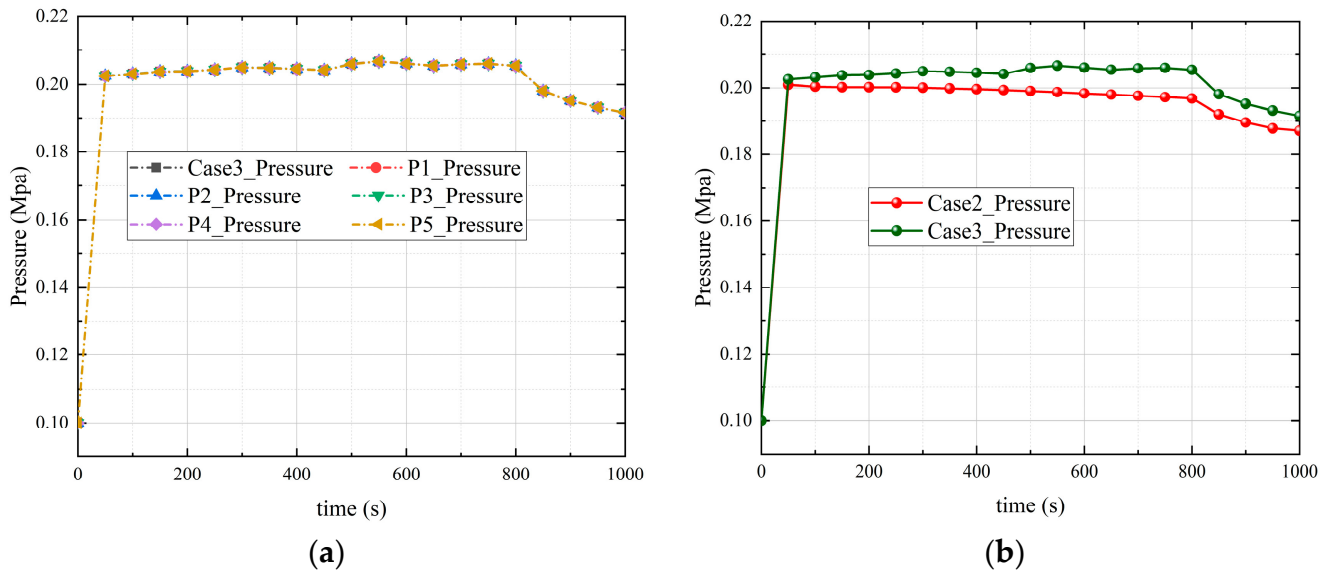


Figure 17. Pressure change in the containment space under different working conditions. (a) Pressure change in Case 3. (b) Average pressure change in Case 2 and Case 3.

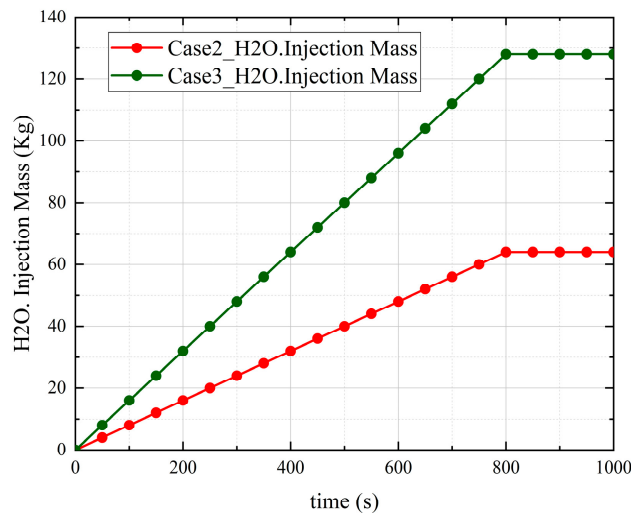


Figure 18. Quality of vapor under different working conditions.

Figure 19 shows the comparison of the average temperature of the containment space under the condition of a small vapor mass flow and the condition of a large vapor mass flow. It can be seen from the figure that during the duration of the accident, compared with the condition of small vapor mass flow, the temperature in the containment space rises faster under the condition of large vapor mass flow, reaching a peak at about 450 s. The reason is that under the condition of constant nozzle size, the initial velocity of the mixed gas injected from the nozzle is larger under the condition of a large vapor mass flow rate, and more high-temperature gas is injected into the containment space at the same time. At the same time, the gas diffusion in the containment space has a larger initial momentum, and the distance that can be moved at the same time is farther, which makes the heat transfer range in the containment space larger so that the temperature in the closed containment space rises faster and higher.

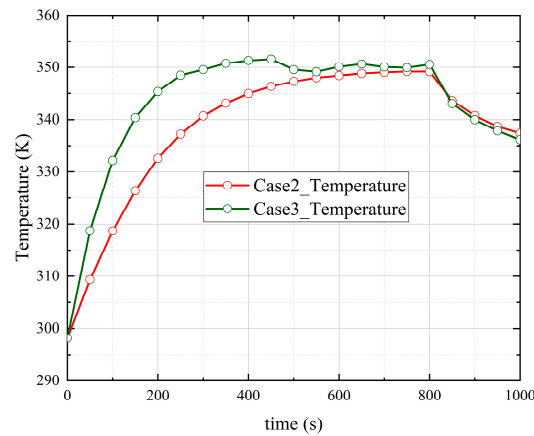


Figure 19. Average temperature change in Case 2 and Case 3.

Figures 20 and 21 are the changes in velocity and hydrogen molar fraction at the P1 measuring point near the nozzle under different working conditions. It can be seen from the figure that in the period of concentrated gas injection, under the premise of constant nozzle size, the velocity at the same time at the P1 measuring point under the condition of a large vapor mass flow is much larger than that under the condition of a small vapor mass flow, which makes the vapor have a stronger entrainment effect on the hydrogen near the nozzle during the injection process, so that the hydrogen molar fraction at the same time at the P1 measuring point near the nozzle is significantly lower.

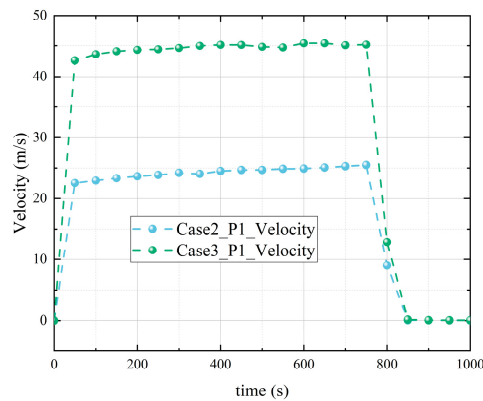


Figure 20. Velocity change at P1 measuring point in Case 2 and Case 3.

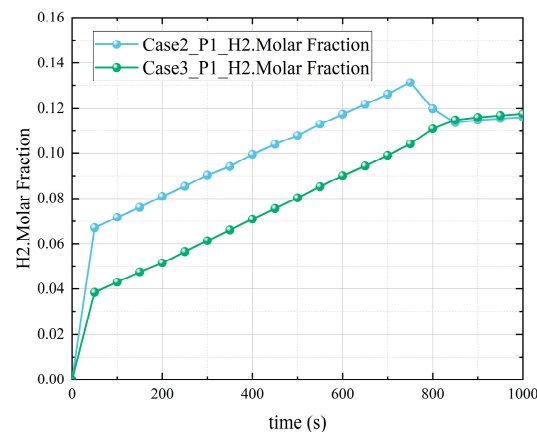


Figure 21. Change of hydrogen concentration at P1 measuring point in Case 2 and Case 3.

Figure 22 is the distribution of the hydrogen molar fraction along the gravity direction at the end of the mixed gas injection under different working conditions. From the diagram, it can be seen that the hydrogen distribution along the gravity direction has a smaller concentration gradient under the condition of a large vapor mass flow rate than that under the condition of a small vapor mass flow rate. The reason for this difference is that, under the condition of the same nozzle size, the mass flow rate of vapor in the mixed gas is larger, which makes the initial momentum of the mixed gas injected into the containment space from the nozzle larger, and the disturbance effect on the gas environment in the containment space is stronger, which promotes the gas mixing in the space, and then makes the hydrogen distribution in the containment space relatively uniform, as shown in Figure 23.

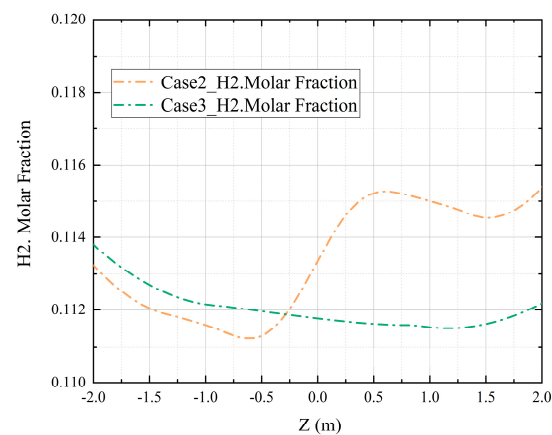


Figure 22. Gravity hydrogen concentration change under different working conditions at $t = 800$ s ($r = 0.15$ m).

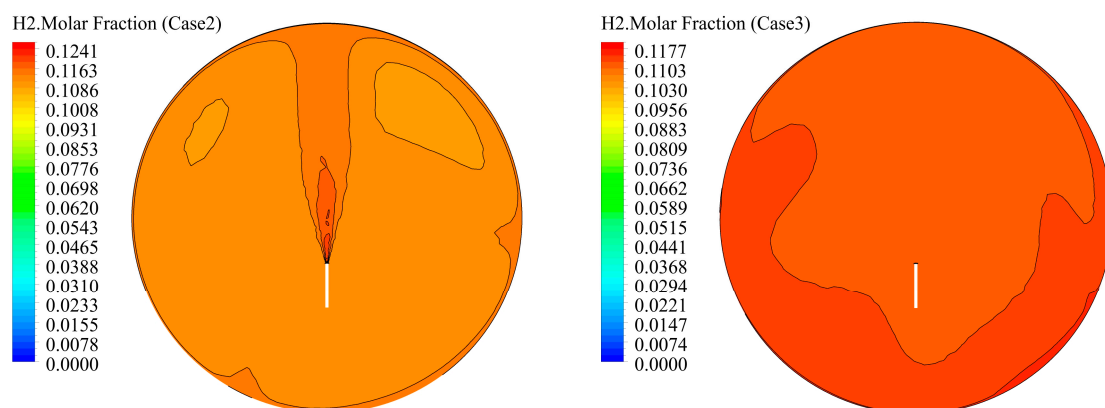


Figure 23. Distribution of hydrogen concentration under different working conditions at $t = 800$ s (left) Case 2; (right) Case 3.

Figure 24 is a Shapiro diagram of hydrogen risk at the P3 measuring point above the nozzle and the P5 measuring point below the break under different working conditions. It can be seen from the figure that in the whole duration of the accident, the time point when the mixed gas concentration at the P3 measuring point and the P5 measuring point reaches the critical concentration of hydrogen combustion is delayed under the condition of large vapor mass flow. The main reason is that under the condition of a large vapor mass flow rate, the mixed gas injected into the containment space stirs the gas environment in the space, greatly promotes the mixing between air, vapor, and hydrogen, and delays the time when the mixed gas concentration in the containment space reaches the critical concentration of hydrogen combustion.

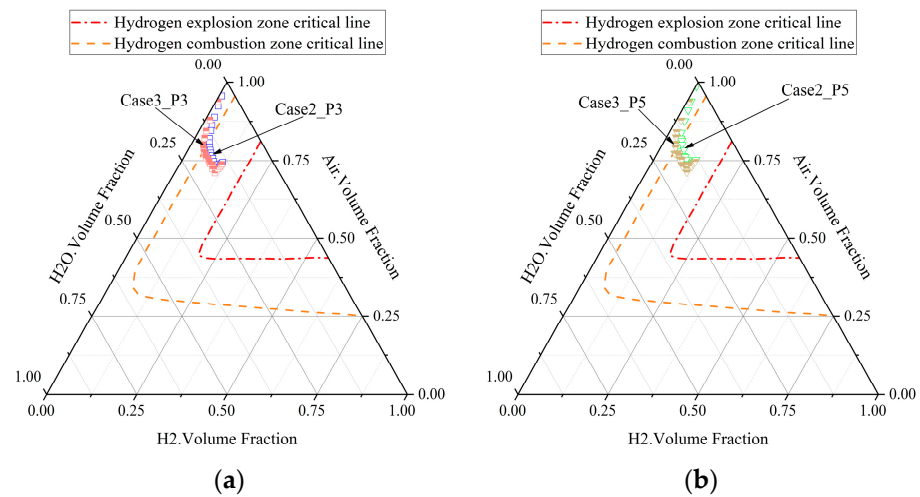


Figure 24. Shapiro diagram at P3 and P5 measuring points under different working conditions. (a) Shapiro diagram at P3 measuring point; (b) Shapiro diagram at P5 measuring point.

5.3. Analysis of the Effect of Vapor Condensation

Figure 25a shows the dynamic changes in the average pressure and pressure at different positions in the containment space under the condition of without vapor condensation. It can be seen from the figure that the average pressure in the containment space under this working condition is consistent with the pressure change trend at each position during the entire accident duration. This phenomenon shows that during a serious accident, even if there is no heat exchange with the external environment in the containment space of the floating nuclear power plant, the pressure response in the containment space is still very rapid, so the pressure at each position in the space quickly reaches the equilibrium state. Compared with the condition without vapor condensation, the average body pressure under the condition with vapor condensation is lower during the whole accident process, and the peak pressure is about 44.99% lower than that without vapor condensation, as shown in Figure 25b. The main reason for this phenomenon is that the high-temperature vapor sprayed from the nozzle will condense when it encounters the cold inner wall of the containment under the condition of vapor condensation, thus reducing the pressure in the containment space.

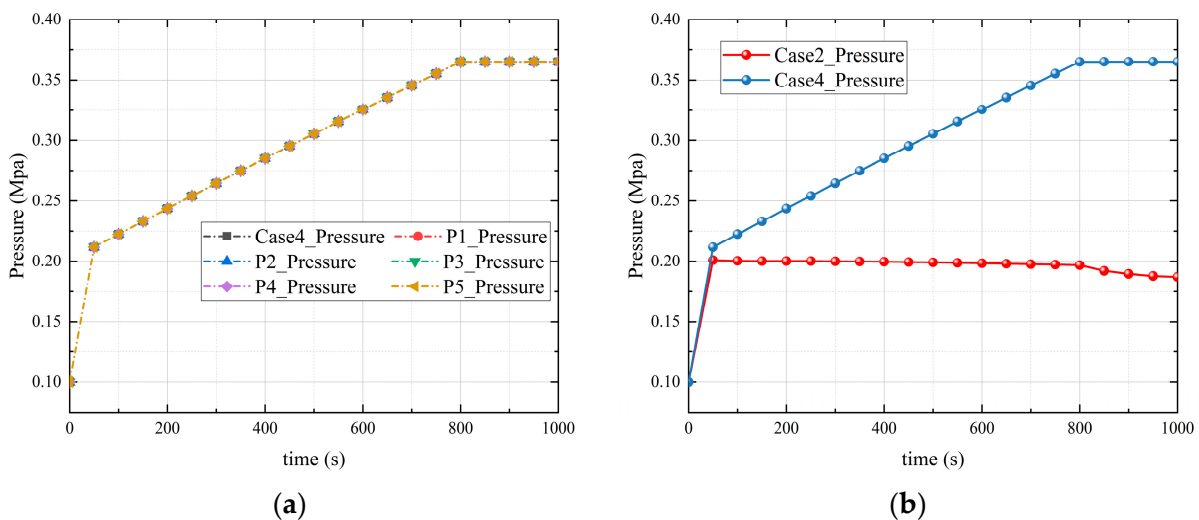


Figure 25. Pressure change in the containment space under different working conditions. (a) Pressure change of Case 4. (b) Average pressure change of Case 2 and Case 4.

Figure 26 is a comparison of the average temperature of the containment space with vapor condensation and without vapor condensation. It can be seen from the figure that during the whole accident process, the temperature in the containment space under the condition of vapor condensation first rises slowly during the gas injection stage, reaching a peak at about 700 s (about 11.47% lower than the peak under the condition of no vapor condensation), and then maintains the peak until the end of the gas injection. The temperature in the containment space slowly decreases to the end of the accident during the standing stage. Under the condition of no vapor condensation, the temperature in the containment space increases continuously during the gas injection stage until the maximum value is reached at the end of the gas injection, and then the value is maintained until the end of the accident. The main reason for this difference is that under the condition of vapor condensation, the high-temperature mixed gas is injected into the closed containment space from the nozzle, and the high-temperature vapor in the mixed gas will condense when it meets the cold inner wall of the containment, which will reduce the temperature in the containment space, while the high-temperature vapor continues to be injected into the containment space from the nozzle, which will increase the temperature in the containment space. At about 700 s, the temperature rise in the vapor ejection and the cooling of the vapor condensation reached an equilibrium state. At this time, the temperature in the containment space reached the peak value, and then the peak value remained unchanged until the end of gas ejection. In the static stage, due to the lack of high-temperature vapor injection, the vapor in the containment space continues to condense, which makes the temperature in the containment space decrease continuously. Under the condition of no vapor condensation, the heat inside the closed containment space cannot be imported into the external environment. The continuous spraying of high-temperature mixed gas will make the temperature in the containment space rise continuously until there is no high-temperature gas spraying, and then the temperature in the containment space remains unchanged during the static stage.

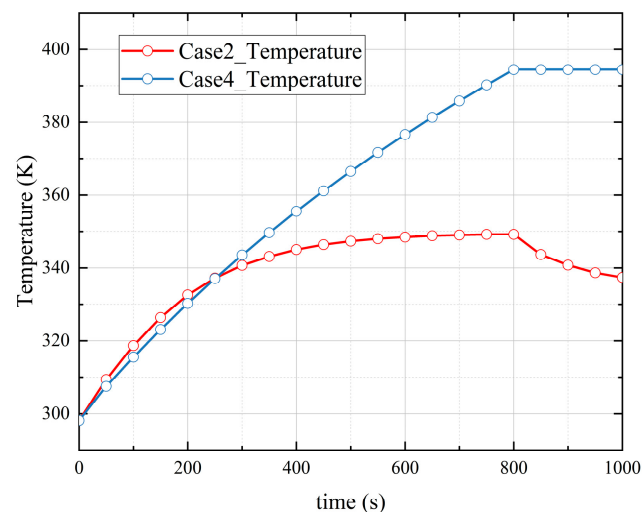


Figure 26. Average temperature change in Case 2 and Case 4.

Figure 27a,b is the dynamic change in hydrogen molar fraction at P3 and P5 measuring points in the containment space under the conditions of vapor condensation and without vapor condensation, respectively. From the diagram, it can be seen that during the whole accident process, the hydrogen molar fraction at the P3 measuring point near the containment wall under the steam condensation condition and the hydrogen molar fraction at the P5 measuring point in the area below the nozzle are higher than the value under the non-steam condensation condition at the same time, and as the accident continues, the difference in hydrogen molar fraction between the two working conditions increases. The main reason is that under the condition of vapor condensation, the high-temperature

vapor in the mixed gas injected into the containment space condenses when it encounters the cold inner wall surface, and the vapor concentration in the mixed gas near the wall surface decreases, so that the concentration of the mixed gas near the wall surface is lower than that of the mixed gas in the mainstream area, thus forming a concentration difference between the near wall surface and the mainstream area. The high-temperature mixed gas in the mainstream area continues to move near the wall under the action of concentration difference, and the vapor in the mixed gas continues to condense so that the hydrogen near the wall continues to accumulate. At the same time, the concentration difference formed by the condensation of the vapor wall will form natural gas convection in the local area of the containment space, which will continuously stir the gas environment in the containment space, promote the gas mixing in the space, and increase the hydrogen concentration below the nozzle. As shown in Figure 28, the streamlined diagram in the containment space under the condition of vapor condensation and no vapor condensation occurred at 1000 s. It can be seen from the figure that the streamline near the inner wall of the containment is denser under the condition of vapor condensation, and the gas flow velocity is higher. This indicates that the gas in the containment space is more agitated under the condition of vapor condensation. The hydrogen distribution cloud diagram of these two conditions at 1000 s shown in Figure 29 intuitively shows the positive effect of vapor condensation on promoting gas mixing in the containment space. Figure 30 shows the distribution of the hydrogen molar fraction along the gravity direction under different working conditions at 1000 s. It can be seen from the map that the axial hydrogen concentration gradient in the containment space is significantly lower under the condition of vapor condensation, which further shows that vapor condensation makes the hydrogen distribution more uniform in the containment space. However, the condensation of vapor will increase the hydrogen concentration in the containment space, which may increase the hydrogen risk in the containment space. As shown in Figure 31, the Shapiro diagram at the P3 measuring point above the nozzle and the P5 measuring point below the nozzle shows that the time point when the mixed gas concentration above the nozzle and below the nozzle reaches the critical concentration of hydrogen combustion is clearly advanced under the condition of vapor condensation.

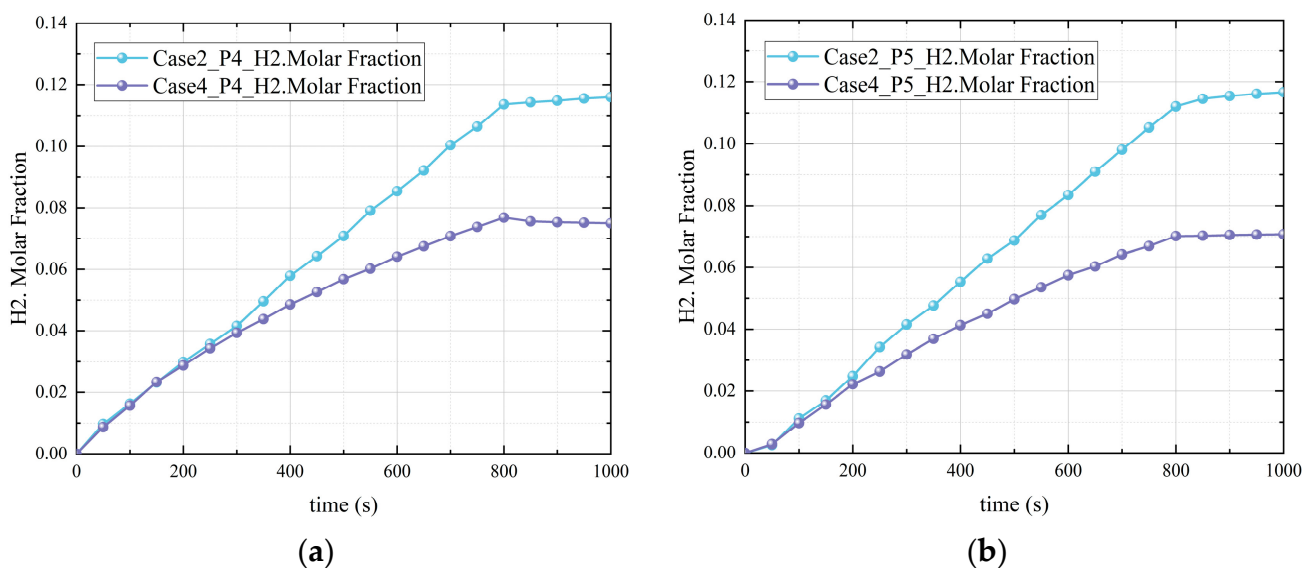


Figure 27. Change in hydrogen concentration at different measuring points under different working conditions. (a) Change in hydrogen concentration at P4 measuring point. (b) Change in hydrogen concentration at P5 measuring point.

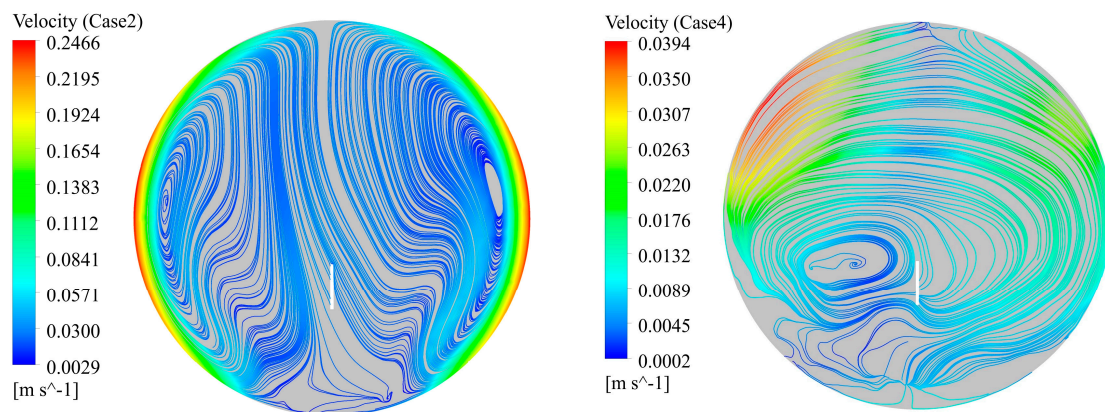


Figure 28. Streamline diagram under different working conditions at $t = 1000$ s (left) Case 2; (right) Case 4.

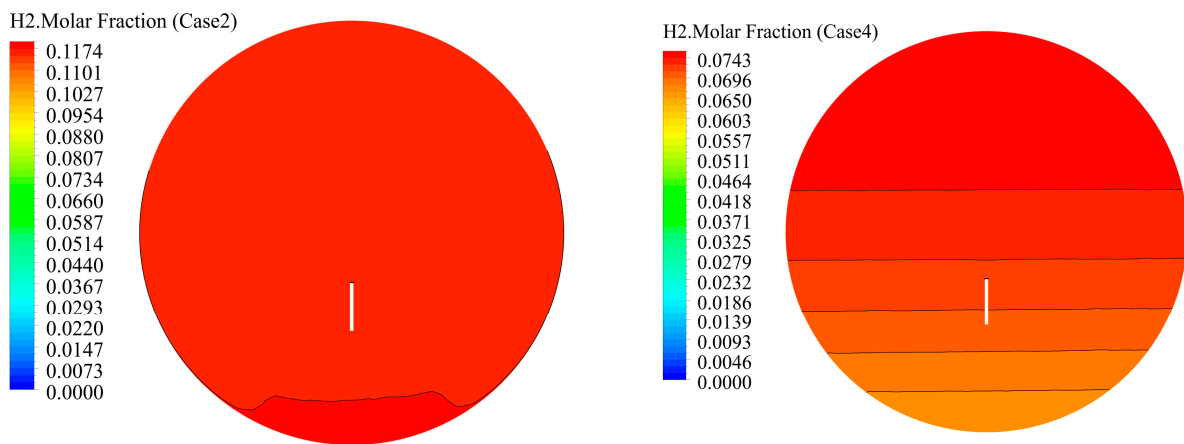


Figure 29. Distribution of hydrogen concentration under different working conditions at $t = 1000$ s (left) Case 2; (right) Case 4.

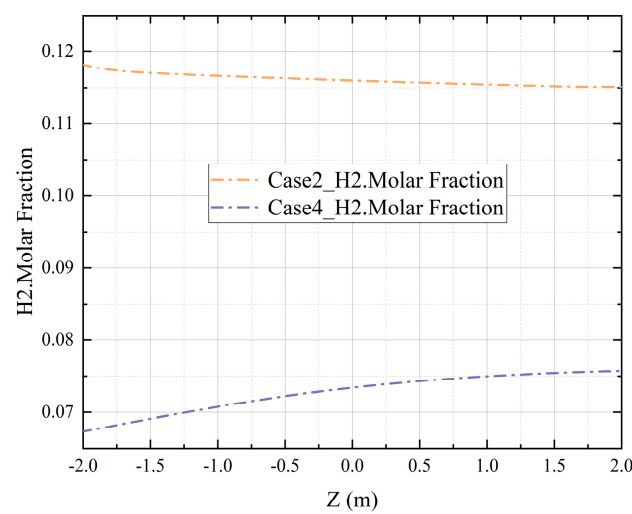


Figure 30. Gravity hydrogen concentration change under different working conditions at $t = 1000$ s ($r = 0.15$ m).

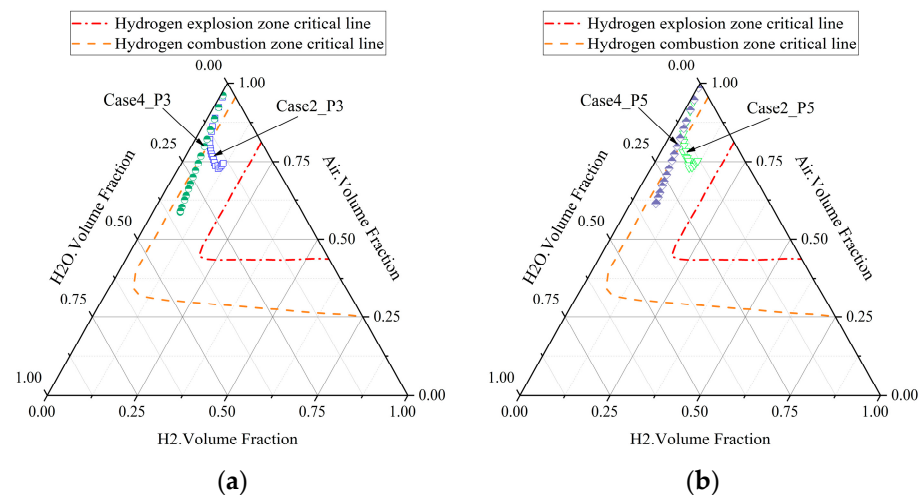


Figure 31. Shapiro diagram at P3 and P5 measuring points under different working conditions. (a) Shapiro diagram at P3 measuring point. (b) Shapiro diagram at P5 measuring point.

6. Conclusions

In this paper, the computational fluid dynamics software CFX is used to simulate the TOSQAN benchmark experiment. The numerical simulation results are compared with the experimental results to verify the applicability of the selected calculation model to simulate the hydrogen distribution in the containment space in the severe accident of marine nuclear power plants. Using the selected calculation model, the numerical simulation of whether there is vapor in the mixed gas sprayed from the nozzle, different vapor concentrations, and the condensation of the vapor wall during the serious accident process induced by a hypothetical loss of coolant accident in a marine nuclear power plant was carried out. The effects of pressure, temperature, hydrogen distribution, and hydrogen risk in the closed containment space were simulated. The analysis results show that:

- (1) The $k - \varepsilon$ turbulence model can be used to simulate the hydrogen distribution in the containment space during the hypothetical severe accident of the marine nuclear power plant.
- (2) During the serious accident of the marine nuclear power plant, the pressure response in the closed finite volume containment space is very rapid. Whether there is vapor, vapor concentration, and vapor condensation has no significant effect on the response speed of the pressure at each position in the containment space to reach the equilibrium state. The condensation of vapor can significantly reduce the pressure in the containment space. Compared to condensation without vapor, the peak pressure is reduced by about 44.99%, which can effectively reduce the risk of high pressure in the containment space.
- (3) The presence of vapor and the increase in vapor concentration will increase the temperature in the containment space during the severe accident of the marine nuclear power plant. The condensation of vapor makes the temperature in the containment space have a peak value during the accident, which is about 11.47% lower than the peak temperature in the containment space without vapor condensation. In the stage without gas injection, the condensation of vapor will make the temperature in the containment space continue to decrease, which can effectively reduce the high-temperature risk in the containment space during a serious accident.
- (4) The presence of vapor and the increase in vapor concentration can reduce the hydrogen concentration near the nozzle during the gas injection process. The reduction effect is significant when there is vapor, which is about 77.17% lower than that without vapor. The condensation of vapor on the wall surface will cause hydrogen to accumulate near the inner wall of the containment and increase the hydrogen concentration near the wall surface.

- (4) The existence of vapor, the increase in vapor concentration, and the condensation of vapor will stir the gas environment in the closed containment space of the marine nuclear power plant, promote the mixing of gas in the containment space during the severe accident, and make the distribution of hydrogen in the containment space tend to be uniform. The presence of vapor and the increase in vapor concentration can reduce the hydrogen risk in the containment space during the accident, but the condensation of vapor will increase the hydrogen concentration in the containment space, which may also increase the hydrogen risk.

Author Contributions: Methodology, J.L. and Y.C.; Software, Z.X. and J.L.; Resources, Y.C.; Writing—original draft preparation, Z.X.; Writing—review and editing, Z.X., J.L., Y.C. and A.L. All authors have read and agreed to the published version of the manuscript.

Funding: This research received no external funding.

Data Availability Statement: The data that support the findings of this study are available on request from the corresponding author. The data are not publicly available due to privacy restrictions.

Conflicts of Interest: The authors declare no conflict of interest.

References

1. Lee, K.; Lee, K.H.; Lee, J.I.; Jeong, Y.H.; Lee, P.S. A new design concept for offshore nuclear power plants with enhanced safety features. *Nucl. Eng. Des.* **2013**, *254*, 129–141. [\[CrossRef\]](#)
2. Santinello, M.; Ricotti, M.E.; Ninokata, H.; Haratyk, G.; Ingremeau, J.J.; Gourmel, V. External heat transfer capability of a submerged SMR containment: The Flexblue case. *Prog. Nucl. Energy* **2017**, *96*, 62–75. [\[CrossRef\]](#)
3. Lee, K.H.; Kim, M.G.; Lee, J.I.; Lee, P.S. Recent Advances in Ocean Nuclear Power Plants. *Energies* **2015**, *8*, 11470–11492. [\[CrossRef\]](#)
4. Buongiorno, J.; Jurewicz, J.; Golay, M.; Todreas, N. The Offshore Floating Nuclear Plant Concept. *Nucl. Technol.* **2016**, *194*, 1–14. [\[CrossRef\]](#)
5. Tong, L.L.; Zou, J.; Cao, X.W. Analysis on hydrogen risk mitigation in severe accidents for Pressurized Heavy Water Reactor. *Prog. Nucl. Energy* **2015**, *80*, 128–135. [\[CrossRef\]](#)
6. Bentaib, A.; Meynet, N.; Bleyer, A. Overview on Hydrogen Risk Research and Development Activities: Methodology and Open Issues. *Nucl. Eng. Technol.* **2015**, *47*, 26–32. [\[CrossRef\]](#)
7. Yanez, J.; Kuznetsav, M.; Souto-Iglesias, A. An analysis of the hydrogen explosion in the Fukushima-Daiichi accident. *Int. J. Hydrog. Energy* **2015**, *40*, 8261–8280. [\[CrossRef\]](#)
8. Peng, C.; Tong, L.L.; Cao, X.W. Numerical analysis on hydrogen stratification and post-inerting of hydrogen risk. *Ann. Nucl. Energy* **2016**, *94*, 451–460. [\[CrossRef\]](#)
9. Wilkening, H.; Ammirabile, L. Simulation of helium release in the Battelle Model Containment facility using OpenFOAM. *Nucl. Eng. Des.* **2013**, *265*, 402–410. [\[CrossRef\]](#)
10. Agrawal, N.; Prabhakar, A.; Das, S.K. Hydrogen Distribution in Nuclear Reactor Containment During Accidents and Associated Heat and Mass Transfer Issues—A Review. *Heat Transf. Eng.* **2015**, *36*, 859–879. [\[CrossRef\]](#)
11. Malet, J.; Porcheron, E.; Vendel, J. OECD International Standard Problem ISP-47 on containment thermal-hydraulics—Conclusions of the TOSQAN part. *Nucl. Eng. Des.* **2010**, *240*, 3209–3220. [\[CrossRef\]](#)
12. Filippov, A.S.; Grigoryev, S.Y.; Tarasov, O.V. On the possible role of thermal radiation in containment thermal-hydraulics experiments by the example of CFD analysis of TOSQAN T114 air-He test. *Nucl. Eng. Des.* **2016**, *310*, 175–186. [\[CrossRef\]](#)
13. Visser, D.C.; Siccama, N.B.; Jayaraju, S.T.; Komen, E.M.J. Application of a CFD based containment model to different large-scale hydrogen distribution experiments. *Nucl. Eng. Des.* **2014**, *278*, 491–502. [\[CrossRef\]](#)
14. Malet, J.; Laissac, R. CFD calculations of stratification build-up tests of light gas in a closed vessel under controlled boundary conditions. *Comput. Fluids* **2015**, *107*, 224–241. [\[CrossRef\]](#)
15. Gupta, S.; Schmidt, E.; von Laufenberg, B.; Freitag, M.; Poss, G.; Funke, F.; Weber, G. THAI test facility for experimental research on hydrogen and fission product behaviour in light water reactor containments. *Nucl. Eng. Des.* **2015**, *294*, 183–201. [\[CrossRef\]](#)
16. Dehbi, A.; Kelm, S.; Kalilainen, J.; Mueller, H. The influence of thermal radiation on the free convection inside enclosures. *Nucl. Eng. Des.* **2019**, *341*, 176–185. [\[CrossRef\]](#)
17. Prabhakar, A.; Agrawal, N.; Raghavan, V.; Das, S.K. Experimental investigations on the evolution of stratified layer of helium in the unventilated vertical cylindrical enclosure of AIHMS facility under wall temperature induced natural convection. *Nucl. Eng. Des.* **2017**, *323*, 367–375. [\[CrossRef\]](#)
18. Prabhakar, A.; Agrawal, N.; Raghavan, V.; Das, S.K. An experimental study on the effect of coaxial circular disk obstacle on helium jet distribution inside the unventilated enclosure of AIHMS facility. *Ann. Nucl. Energy* **2018**, *116*, 347–359. [\[CrossRef\]](#)

19. Filippov, A.S.; Grigoryev, S.Y.; Tarasov, O.V.; Iudina, T.A. Cfd Simulation of Panda And Mistra Cooler Tests of Ercosam-Samara Project. In Proceedings of the 22nd International Conference on Nuclear Engineering (ICONE22), Prague, Czech Republic, 7–11 July 2014; Amer Soc Mechanical Engineers: New York, NY, USA, 2014.
20. Bakhmet'ev, A.M.; Bol'shukhin, M.A.; Kamnev, M.A.; Khizbullin, A.M.; Tyurikov, O.V. Computational and Experimental Studies of Mixing of a Light Gas in the ERCOSAM-SAMARA Projects. *Atom. Energy* **2017**, *123*, 1–9. [[CrossRef](#)]
21. Fernandez-Cosials, M.K.; Jimenez, G.; Lopez-Alonso, E. Analysis of a gas stratification break-up by a vertical jet using the GOTHIC code. *Nucl. Eng. Des.* **2016**, *297*, 123–135. [[CrossRef](#)]
22. Kelm, S.; Lehmkuhl, J.; Jahn, W.; Allelein, H.J. A comparative assessment of different experiments on buoyancy driven mixing processes by means of CFD. *Ann. Nucl. Energy* **2016**, *93*, 50–57. [[CrossRef](#)]
23. Povilaitis, M.; Urbonavicius, E.; Rimkevicius, S. Validation of special nodalisation features for lumped-parameter injection modelling based on MISTRA facility tests from ISP-47 and SARNET. *Nucl. Eng. Des.* **2014**, *278*, 86–96. [[CrossRef](#)]
24. Visser, D.C.; Houkema, M.; Siccama, N.B.; Komen, E.M. Validation of a FLUENT CFD model for hydrogen distribution in a containment. *Nucl. Eng. Des.* **2012**, *245*, 161–171. [[CrossRef](#)]
25. Kim, J.; Jung, E.; Kang, S. Large eddy simulation of hydrogen dispersion from leakage in a nuclear containment model. *Int. J. Hydrogen Energy* **2015**, *40*, 11762–11770. [[CrossRef](#)]
26. Liu, F.; Sun, Z.N.; Cao, B.Y.; Bian, H.Z.; Ding, M. Numerical investigations on the component separation phenomenon and transport behavior of steam-air-hydrogen mixture induced by condensation. *Int. J. Therm. Sci.* **2022**, *172*, 16. [[CrossRef](#)]

Disclaimer/Publisher's Note: The statements, opinions and data contained in all publications are solely those of the individual author(s) and contributor(s) and not of MDPI and/or the editor(s). MDPI and/or the editor(s) disclaim responsibility for any injury to people or property resulting from any ideas, methods, instructions or products referred to in the content.